Hybridization of ionic levels at metal surfaces

P. Kürpick* and U. Thumm
J. R. Macdonald Laboratory, Department of Physics, Kansas State University, Manhattan, Kansas 66506-2604
(Received 20 October 1997)

We investigated the hybridization of He^+, Li^{2+}, and Be^{3+} ionic levels and the creation of surface resonances for nuclear charges $Z=2$, 3, and 4 near an Al surface. Starting from a two-center basis set expansion with hydrogenic wave functions on the ion site and jellium wave functions in the metal half space, we calculate the self-energy for ion-surface system in the fixed-ion approximation. We obtain convergence by using a rather small set of bound ionic states. This ideally suits this method for the generation of adiabatic basis states that can be used in time-dependent close-coupling calculations for slow ion-surface collisions. We compare our resonance energies and widths with other theoretical approaches, discuss electronic density profiles, and analyze resonances in terms of Stark states. [S1050-2947(98)01109-3]

PACS number(s): 34.50.Dy, 31.15.−p, 34.70.+e, 61.80.Jh

I. INTRODUCTION

Detailed understanding of the dynamics of ion-metal surface interactions has been a primordial experimental and theoretical topic in the last decade. Experimentally, the interaction of single ions with metal surfaces has been investigated in various ways. Charge-state distributions of highly charged ions scattered from a single-crystal surface [1] and accelerations of an incoming ion due to the image charge [2,3] have been observed. The existence of hollow-atom states formed by resonant electron capture has been confirmed through high-resolution Auger electron spectroscopy measurements [4]. These experiments ask for *ab initio* calculations investigating the neutralization and ionization of ions approaching a metal surface.

From a theoretical point of view several studies focusing on one-electron effects, which are supposed to be dominant at ion-surface distances $D>5$ a.u., can be found in the literature: Early perturbative calculations go back to Gadzuk [5] and Remy [6]. Scattering calculations in first- and second-order impulse approximation have been performed by Thumm and Briggs [7–10]. More recently systematic investigations of closed-form expressions for the transfer matrix elements and universal scaling properties for transition rates of Rydberg states were derived by Wille [11,12] and Kürpick and Thumm [13]. Besides these perturbative approaches, solutions of the time-dependent and time-independent Schrödinger equation have been attained at various levels of approximation. Using a two-center expansion together with the self-energy concept, Burgdörfer *et al.* [14,15] studied the hybridization of the $(n=2)$ manifold for hydrogen interacting with an Al surface. Kürpick *et al.* performed converged self-energy calculations up to $n=6$ for hydrogen interacting with an Al surface [16,17]. In the self-energy formalism, the expansion coefficients of the substrate-centered basis are formally eliminated such that a restricted set of close-coupling equations in the subspace of atomic basis functions is obtained in which the coupling to the substrate appears as a complex potential, the self-energy. Borisov *et al.* [18–20] applied the coupled-angular mode (CAM) method to the broadening of atomic levels near metal surfaces for ions up to O^{7+}. The CAM method essentially views atomic resonances as scattering resonances corresponding to elastic scattering of conduction-band electrons by the ionic potential. A different approach has been undertaken by Nordlander *et al.* and Deutscher *et al.* by means of the complex scaling method [21–25], which involves a complex non-Hermitian Hamiltonian. Deutscher *et al.* [23–25] focused on $(n=1,2)$-surface resonances in H-Al surface interactions while Nordlander *et al.* [21,22] calculated shifts and widths of Rydberg states up to $n=10$ for various ions and surfaces. Furthermore, level positions and widths for H atoms in front of an Al surface have been obtained by Martin and Politis [26] within a ''stabilized'' multicenter-Gaussian expansion method.

In this paper we present a large-scale application of the two-center expansion method with hydrogenic states on the ion site and jellium states for the metal half space. We solve the close-coupling equations by eliminating the explicit dependence on the jellium states. This elimination leads to a complex non-Hermitian self-energy matrix. The subsequent diagonalization of the self-energy matrix yields the shifted energies and widths of ion-surface resonances formed when the ion velocity perpendicular to the surface is small compared to the electron velocity. This adiabatic picture shows a strong hybridization of ionic levels similar to the well-known Stark mixing of hydrogenic levels. We emphasize that the resonance widths are associated with either the resonant filling of an ionic level (resonant capture) or with the resonant loss of an ionic electron into the unoccupied part of the metal conduction band. Which of these two cases applies depends on the initial occupation of ionic and surface electronic states. At zero temperature and for resonance energies below the Fermi level of the surface, the resonance widths describe resonant capture into states about a nucleus of charge Z; for resonance energies above the Fermi level they correspond to resonant loss rates.

We have organized this paper of follows. In Sec. II we present a short summary of the close-coupling expansion with emphasis on the self-energies. The actual evaluation of

*Present address: SAP-AG, Neurottstrasse 16, 69190 Walldorf, Germany.

 © 1998 The American Physical Society

the self-energy is done by decomposing the full Hamiltonian for the ion-surface system into channel Hamiltonians corresponding to unperturbed conduction-band states and discrete hydrogenic states, respectively. Results for the case of various ions interacting with an Al surface with emphasis on the dependence of surface resonances on the hydrogenic n- and m-quantum number are discussed in Sec. III. Section IV gives a summary of our paper in which atomic units are used throughout.

II. THEORY

In this section, we briefly present a derivation of the complex non-Hermitian self-energy formalism using two mutually nonorthogonal basis sets within the independent particle model. Details of the formulation and a thorough test on the H-Al system have been published elsewhere [16].

The self-energy method first applied to ion-surface interactions by Burgdörfer *et al.* [14,15] starts from the time-dependent Schrödinger equation

$$i|\dot{\Psi}(t)\rangle = H(t) \ \ |\Psi(t)\rangle \ \ , \tag{2.1}$$

in which the Hamiltonian $H(t)$ is time dependent due to the motion of the ion along a prescribed classical trajectory (we adopt a reference frame in which the metal is at rest). The total one-electron Hamiltonian $H(t)$ is taken in the form

$$H(t) = T + V_S + V_C^{>}(t), \tag{2.2}$$

where T is the kinetic energy. The surface potential V_S includes both the electronic self-image potential $V_e^{(i)}(z)$ and the nuclear image potential $V_C^{(i)}(\vec{r};D)$ acting on the electron,

$$V_S(z) = \begin{cases} -V_0, & z < z_0 \\ V_e^{(i)}(z) + V_C^{(i)}(z;D), & z \geqslant z_0, \end{cases} \tag{2.3}$$

where $z_0 > 0$ is determined from the condition

$$V_e^{(i)}(z_0) + V_C^{(i)}(z_0;D) = -V_0 \tag{2.4}$$

and $-V_0$ is the energy of the lower conduction-band limit with respect to the ionization threshold. The potential $V_C^{>}$ is the potential of the ion core, cut off at the surface in order to allow for the complete screening of the core potential inside the metal. The potentials

$$V_e^{(i)}(z) = -\frac{1}{4z}\,\Theta(z) \tag{2.5}$$

and

$$V_C^{(i)}(\vec{r};D) = \frac{Z}{|\vec{r} + D\hat{e}_z|} \ \ \Theta(z) \approx V_C^{(i)}(z;D) = \frac{Z}{|z+D|} \ \ \Theta(z) \tag{2.6}$$

are the classical image potentials induced by the active electron and by the ion core, respectively. As can be seen from Eq. (2.6) we approximate the nuclear image potential by its value on the z axis, therefore slightly overestimating its influence. In a previous article [16] we have compared the surface potential according to Eq. (2.3) with the commonly used Jennings potential [28] and found minor deviations, as can be also seen in Sec. III below.

The function $|\Psi(t)\rangle$ is expanded as

$$|\Psi(t)\rangle = \sum_{j=1}^{N} a_j(t) \ \ |\psi_j(t)\rangle + \int_{k \leqslant k_{\max}} d\vec{k} \ \ \rho(\vec{k}\,) \ \ b_{\vec{k}}(t) \ \ |\phi_{\vec{k}}\rangle, \tag{2.7}$$

where the basis functions $|\psi_j(t)\rangle$ are eigenfunctions of the stationary Hamiltonian

$$H_f = T + V_C \tag{2.8}$$

and are centered at the ion site. The basis functions $|\phi_{\vec{k}}\rangle$ are eigenfunctions to the step potential V_{step} with wave vector $\vec{k}$ and energy $\epsilon_{\vec{k}}$. $\rho(\vec{k}\,)$ is the corresponding (free-electron) density of states. We restrict the set of basis functions $\{|\phi_{\vec{k}}\rangle\}$ to functions localized in the metal half-space, so that the maximum wave number is given by $k_{\max} = \sqrt{2V_0}$. The function $|\phi_{\vec{k}}\rangle$ are eigenfunctions of the Hamiltonian

$$H_i = T + V_{\text{step}} \ \ . \tag{2.9}$$

We decompose the total Hamiltonian (2.2) into initial and final channel Hamiltonians according to

$$H = H_i + V_i = H_f + V_f. \tag{2.10}$$

Taking the potential step in V_{step} at z_0, initial and final channel perturbation potentials follow as

$$V_i = \begin{cases} 0, & z < z_0 \\ V_C + V_e^{(i)} + V_C^{(i)}, & z \geqslant z_0 \end{cases} \tag{2.11}$$

and

$$V_f = \begin{cases} -V_0 - V_C, & z < z_0 \\ V_e^{(i)} + V_C^{(i)}, & z \geqslant z_0 \ \ . \end{cases} \tag{2.12}$$

In all applications shown subsequently we retain the Coulomb potential in the initial channel perturbation (2.11) and neglect the image potentials in V_i. With respect to the final channel potential V_f, we do not include V_C in Eq. (2.12).

Inserting the expansion (2.7) into the Schrödinger equation (2.1) and projecting onto the basis functions, we obtain a set of close-coupling equations. The fixed-ion approximation [14–16] corresponds to the static limit in which the ion is at rest at a distance D in front of the surface. Accordingly, the Hamiltonian H is independent of time and depends only parametrically on D. In this case, the set of close-coupling equations can be converted, by means of a Laplace transformation in the variable s, into a system of algebraic equations for the transformed expansion coefficients $\tilde{a}_j(s)$ and $\tilde{b}_{\vec{k}}(s)$. If the direct couplings among the metal states are neglected, the coefficients $\tilde{b}_{\vec{k}}(s)$ can be eliminated from the algebraic system. The resulting linear system of equation for the ionic coefficients $\tilde{a}_j(s)$, corresponding to initial conditions where the Fermi sea of metal electrons is completely filled and the ionic levels are unoccupied, reads

$$\sum_{j'} [is\,\delta_{jj'} - \mathcal{S}_{jj'}(s)]\ \tilde{a}_{j'}(s) = i \int_{k \le k_F} d\vec{k}\ \ \rho(\vec{k}\,)\ \ \frac{W_{j\vec{k}}}{is - \epsilon_{\vec{k}}}\ , \tag{2.13}$$

where k_F is the Fermi momentum of the metal, and $\mathcal{S}(s)$ is the complex (static) self-energy. The self-energy describes the effective interaction that governs the dynamics in the ionic space in the presence of couplings to the metal states. The initial occupations of conduction-band states that are filled up to the Fermi level appear on the right-hand side of the above equation, but are not included in the self-energy. Many-body effects, in particular the Pauli-exclusion principle, are not incorporated in the self-energy. As a consequence, its imaginary part (the resonance width) can be seen as related to either the resonant capture rate or the rate of resonant loss into empty conduction-band states. The position of the resonance energy, i.e., the real part of the self-energy, relative to the Fermi level, determines which states are inaccessible due to ''Pauli blocking'' and thus determines the possible direction of the transfer process. When expressing s in terms of the real energy variable ω by $s = -i\ \omega + \eta$, the matrix elements of $\mathcal{S}(\omega)$ are given by

$$\mathcal{S}_{jj'}(\omega) = \epsilon_j \delta_{jj'} + F_{jj'} + \mathrm{P} \int_{k \le k_{\max}} d\vec{k} \rho(\vec{k}\,)\ \ \frac{[(\epsilon_{\vec{k}} - \omega)\ N_{j\vec{k}} + W_{j\vec{k}}]\ \ [(\epsilon_{\vec{k}} - \omega)\ N^*_{j'\vec{k}} + W^*_{j'\vec{k}}]}{\omega - \epsilon_{\vec{k}}}$$

$$- i\pi \int_{k \le k_{\max}} d\vec{k}\ \ \rho(\vec{k}\,)\ \ W_{j\vec{k}}\ \ W^*_{j'\vec{k}}\ \ \delta(\omega - \epsilon_{\vec{k}})\ \ , \tag{2.14}$$

where P denotes the principal part and η is a positive infinitesimal guaranteeing (Siegert) resonance boundary conditions. The initial-channel transfer matrix elements $W_{j\vec{k}}$, overlap matrix elements $N_{j\vec{k}}$, and the final-channel distortion matrix elements $F_{jj'}$ are defined as

$$W_{j\vec{k}} = \langle \psi_j | V_i | \phi_{\vec{k}} \rangle, \tag{2.15}$$

$$N_{j\vec{k}} = \langle \psi_j | \phi_{\vec{k}} \rangle, \tag{2.16}$$

and

$$F_{jj'} = \langle \psi_j | V_f | \psi_{j'} \rangle\ \ . \tag{2.17}$$

For a detailed study of these matrix elements, we refer to Refs. [11–13]. The (off-shell) principal-part term in Eq. (2.14) describes indirect couplings between ionic states due to virtual transitions into the conduction band, while the (on-shell) term proportional to $i\pi$ (''width term'') describes real transitions into the conduction band and gives rise to the resonance broadening of the dressed ionic levels. By subsequently diagonalizing the self-energy matrix (2.14) we obtain complex eigenvalues $\tilde{\omega}_\mu(D)$, and eigenvectors $|\phi_\mu(D)\rangle$, where μ collectively denotes the quantum numbers characterizing the states. The complex eigenvalues $\tilde{\omega}_\mu(D)$ relate to the energetic shifts $E_\mu(D)$ and widths $\Gamma_\mu(D)$ according to

$$E_\mu(D) = \mathrm{Re}\ \tilde{\omega}_\mu(D), \tag{2.18}$$

$$\Gamma_\mu(D) = -2\ \mathrm{Im}\ \tilde{\omega}_\mu(D). \tag{2.19}$$

The nonlinear eigenvalue problem (2.13) is approximately solved by evaluating the matrix elements $\mathcal{S}_{jj'}(\omega)$ at

$$\omega = \frac{\epsilon_j + \epsilon_{j'}}{2}. \tag{2.20}$$

We represent the resonance wave functions as hybrid wave functions that are given as linear combinations of ionic orbitals of a particular magnetic quantum number m according to

$$|\phi_\mu(D)\rangle = \sum_{j=1}^{N} a_{\mu,j}(D) |\psi_j\rangle. \tag{2.21}$$

III. NUMERICAL RESULTS AND DISCUSSION

We have calculated level positions, level widths, and electronic charge densities of ion-surface states that form if a nucleus of charge $Z = 2$, 3, and 4 is placed at a given distance in front of an Al surface. The Al surface is characterized by the potential depth $V_0 = 0.585$ a.u. and the work function $W = 0.15$ a.u. Resonance states with larger binding energies, between $-V_0$ and $-W$, may be filled by resonant tunneling. At large ion-surface distances the asymptotic $n = 2$ and $n = 3$ manifolds of He^+, the $n = 3$ to $n = 5$ manifolds of Li^{2+}, and the $n = 4$ to $n = 7$ manifolds of Be^{3+} are in resonance with the filled part of the Al conduction band. As can be seen from our Hamiltonian (2.2), the ion-surface system exhibits a cylindrical symmetry with respect to the z axis perpendicular to the surface. Therefore the m quantum number is conserved and different m manifolds can be investigated separately. We will mainly investigate the $m = 0$ manifold but show that $m \neq 0$ manifolds have a very similar behavior. In a previous paper [16] the convergence of our method, with respect to the size of the ionic basis set was studied in detail and the nth manifold was found to be converged if the $n-1$ and $n+1$ manifolds are included in the basis set. This rule holds as long as the very strong interaction of ionic states with the metal surface, which sets in at ion-surface distances below the classical orbit radius $\langle r \rangle = n^2/Z$, leads to a strong promotion across all higher n manifolds. The self-energy method therefore allows us to obtain accurate energies and widths of

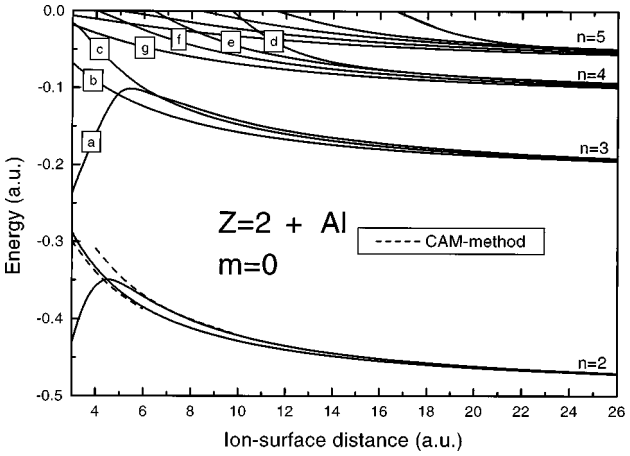

FIG. 1. Energies of the $m=0$ resonances states of the asymptotic ($n=2$) to ($n=5$) manifolds for a nuclear charge $Z=2$ near an Al surface. The labels $a-g$ refer to the widths shown in Fig. 2. The dashed lines show results by Borisov *et al.* [20].

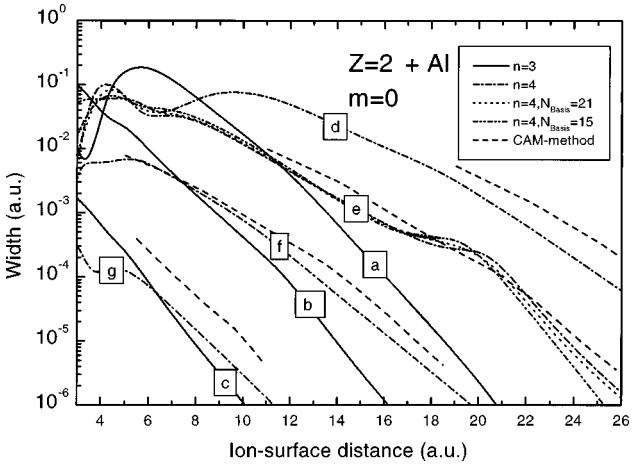

FIG. 2. Widths of the $m=0$ resonances states of the asymptotic ($n=3$) and ($n=4$) manifolds for a nuclear charge $Z=2$ near an Al surface. The labels $a-g$ refer to the energies shown in Fig. 1. The dashed lines show results by Borisov *et al.* for the $n=4;m=0$ manifold [20].

resonance states while using a small set of bound ionic orbitals.

A. $Z=2$ + Al

Figure 1 shows for the case of a nuclear charge $Z=2$ near an Al surface converged resonance energies of all $m=0$ states emanating from the asymptotic $n=2$ to $n=5$ manifolds of He^+. The ionic basis set in the calculation was built up by the $n=1$ to $n=8$ manifolds, therefore including 36 states. At large ion-surface distances all states exhibit a monotonic upward shift due to the nuclear image potential. At close ion-surface distances the interaction of the ionic states with the metal surface through the final-channel potential matrix elements [see Eq. (2.17)] leads to an energetic downward shift of those resonance states that strongly overlap with the surface as, for example, resonance *a*. The dashed lines show results by Borisov *et al.* obtained using the CAM method [20]. The agreement is good down to about $D=3$ a.u. for the state whose probability distribution mainly points towards the vacuum while discrepancies occur below $D=6$ a.u. for the state that is primarily oriented towards the metal surface. These discrepancies are due to the different choices of the nuclear image potential near the surface. Borisov *et al.* keep the full nuclear image potential down to $z=0$ while in our calculations the nuclear image potential is turned off when the sum of the nuclear image potential and electronic self-image potential add up to the value of $-V_0$. This happens for $z>0$ [see Eq. (34) in Ref. [16]], and weakens the influence of the nuclear image potential on the atomic resonances.

Figure 2 shows the widths of the asymptotic $n=3$ and $n=4$ manifolds. The designation $a-c$ refers to the energies of the $n=3$ manifold shown in Fig. 1 while the designation $d-g$ marks the levels of the asymptotic $n=4$ manifold. To exhibit how convergence is achieved within a small set of ionic basis functions, we have also plotted in Fig. 2 the width of the resonance state *e* obtained while using a basis set spanned by the $n=1$ to $n=6$ states (21 basis functions) and the $n=1$ to $n=5$ states (15 basis functions). The convergence is rapidly achieved and the accuracy far better than the physical accuracy of the potentials used in the Hamiltonian (2.2). Within a given *n* manifold resonance states have very distinct widths and states of the same *n* manifold generally tend to have the same exponential slope at large ion-surface distances. Exceptions to this rule are obvious for the resonance state denoted with *e*. Due to adiabatic couplings, the exponential slope of its width changes in the ion-surface distance range of 18 to 20 a.u. The dashed lines show results by Borisov *et al.* [20] for the $n=4;m=0$ manifold. Their widths for most ion-surface distances tend to be a factor of 2–4 larger than our results. This behavior is also observed for the state with low width in the $Z=3$–Al system as discussed below. Although not as pronounced as in our calculations, the results by Borisov *et al.* also exhibit a shoulder and change of slope for the width of the resonance state denoted as *e*.

An appropriate way to analyze the behavior of resonance states is to express the resonance wave function as a linear combination of Stark states

$$|\phi_{\mu,m}(D)\rangle=\sum_{n,k} c_{\mu,n,k,m}(D)|\xi_{n,k,m}\rangle, \tag{3.1}$$

where the parabolic Stark states are given as linear combinations of spherical hydrogenic orbitals and the coefficients are the Clebsch-Gordan coefficients [29]

$$|\xi_{n,k,m}\rangle=\sum_{l=0}^{n-1}\begin{pmatrix}(n-1)/2 & (n-1)/2 & l\\ (m+k)/2 & (m-k)/2 & m\end{pmatrix}|\psi_{nlm}\rangle. \tag{3.2}$$

The comparison of nonperturbative widths obtained by the CAM method with first-order widths calculated for parabolic Stark states by Borisov and Wille [19] showed that, at large ion-surface distances, Stark states are good approximations to the resonance wave functions. Given our axis of quantization perpendicular to the surface, the largest positive electric quantum number *k* corresponds to a Stark state pointing towards the surface therefore exhibiting a large width, whereas

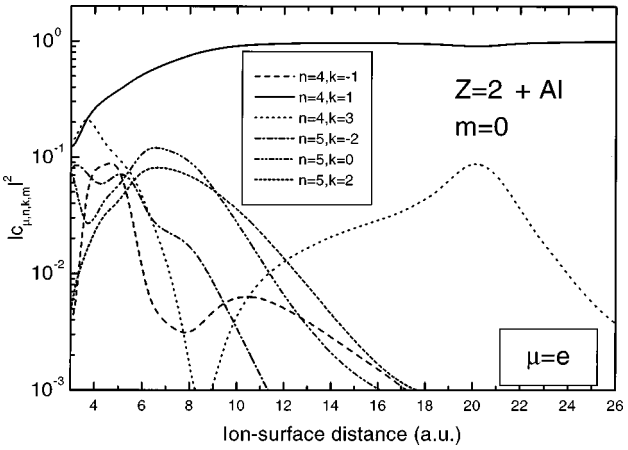

FIG. 3. Square amplitudes of the parabolic Stark state contributions to the resonance state denoted as *e* in Figs. 1 and 2.

the largest negative electric quantum number k corresponds to a Stark state pointing towards the vacuum and has a small width. Figure 3 shows the six largest square amplitudes according to Eq. (3.1) for the resonance state denoted as *e* in Figs. 1 and 2. The resonance state *e* tends for large ion-surface distances towards the $n=4$, $k=1$ parabolic state. Comparing Figs. 2 and 3, one sees that the width changes its slope at approximately 20 a.u. where the resonance state *e* shows the strongest admixture of the *large-width* $n=4$, $k=3$ parabolic state.

B. $Z=3$ + Al

Our results for a charge $Z=3$ near an Al surface can be compared with nonperturbative calculations by Borisov *et al.* [20] and perturbative calculations by Borisov and Wille [19]. Figure 4 shows the converged energy shifts of $m=0$ resonance states emerging out of the asymptotic $n=5$ to $n=7$ manifold while using an ionic basis set spanned by the $n=3$ to $n=9$ manifolds. The dashed lines in Fig. 5 show results by Borisov *et al.* [20] for the $n=5;m=0$ manifold obtained using the CAM method. The discrepancies between

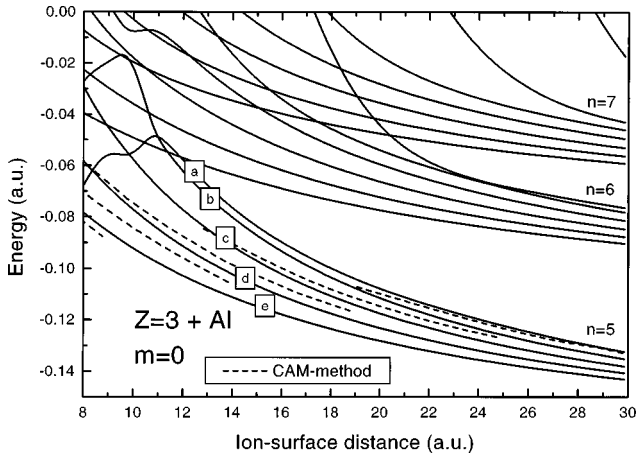

FIG. 4. Energies of the $m=0$ resonances states of the asymptotic $n=5$ to $n=7$ manifolds for a nuclear charge $Z=3$ near an Al surface. The dashed lines show results by Borisov *et al.* for the $n=5;m=0$ manifold [20]. The labels $a-e$ refer to the widths shown in Fig. 5.

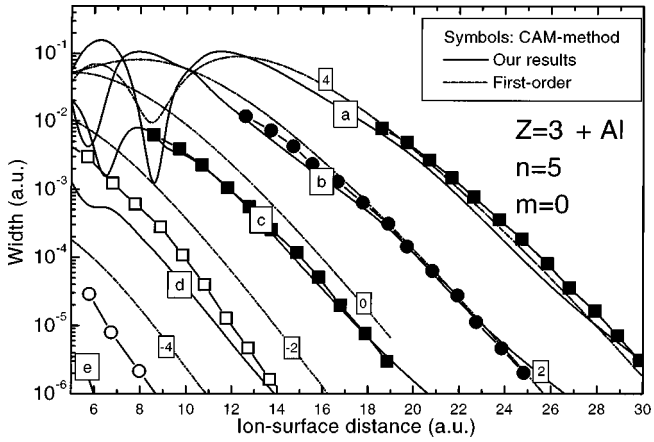

FIG. 5. Widths of the $n=5;m=0$ resonances states for a nuclear charge $Z=3$ near an Al surface. The symbols show results obtained by Borisov and Wille using the CAM method [19]. The dash-dotted lines are first-order calculations in the parabolic (Stark) basis denoted by their electric quantum number by Borisov and Wille [19]. The labels $a-e$ refer to the energies shown in Fig. 4.

the CAM results and our self-energy calculations originate from the approximation to the nuclear image potential in our approach, which leads to an overestimation of its strength and therefore to a somewhat stronger upward shift of all levels.

Figure 5 presents the converged widths of resonance states formed near an Al surface out of the asymptotic $n=5$ manifold of Li^{2+} states. The symbols in Fig. 5 refer to the non-perturbative CAM results obtained by Borisov and Wille [19]. Although these authors use the more refined Jennings potential [28] to represent the metal surface, our widths tend to agree very well with the CAM results for the three states exhibiting the largest widths. The general trend in the agreement between the CAM results and our results can be understood by looking at the wave function of the resonance states. Those resonances having a rather large width strongly overlap with the surface potential barrier and therefore average over large portions of space. In contrast, those states having a small width exhibit a very weak overlap with the surface and are therefore more sensitive to details of the surface potential. Since Borisov and Wille [19] used the Jennings potential in their CAM calculations, their widths tend to be larger because the surface potential is smeared out along the z axis perpendicular to the surface. This leads to metal states in which more probability density *leaks* into the vacuum as compared to our jellium potential [see Eq. 2.3].

In Fig. 5 we also plotted first-order widths obtained from parabolic (Stark) states [19], which are denoted by the electric quantum number $k=-4,\ldots,4$. These first-order calculations rely on the same surface potential as our nonperturbative calculations. The widths extracted from these first-order results tend to be bigger than both nonperturbative approaches especially for resonance states with a small width. One should keep in mind that states with small widths do not contribute significantly to the neutralization process in any ion-surface encounter. Errors in their widths are therefore of little relevance to the overall physical behavior. To get a better understanding of the deviation of the first-order Stark results from both nonperturbative results, we have per-

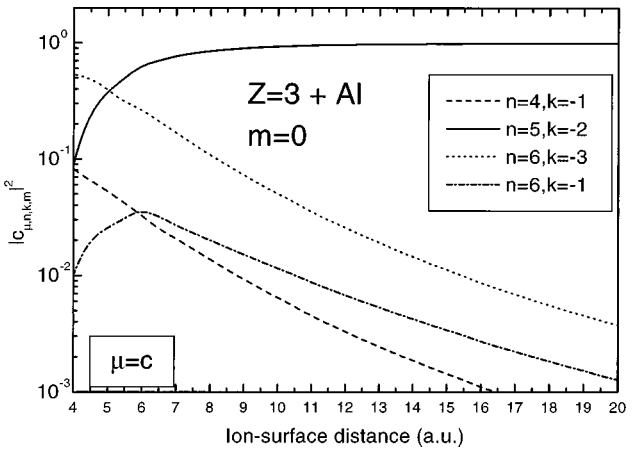

FIG. 6. Square amplitudes of the parabolic Stark state contributions to the resonance state denoted as c in Figs. 4 and 5.

formed, as for the case of $Z=2$, an analysis of our resonance states in terms of Stark states. As an example Fig. 6 shows the four largest square amplitudes of Stark states contributing to the resonance state denoted as c in Figs. 4 and 5. Its width shows a deviation from the first-order Stark calculation while both nonperturbative results agree very well among each other (Fig. 5). Although the resonance state c tends for large ion-surface distances towards the parabolic state with quantum numbers $n=5$, $k=-2$ it has a contribution of the $n=6$, $k=-3$ parabolic state that grows to about 53% at an ion-surface distance of 4 a.u. The $n=6$, $k=-3$ parabolic state is expected to have a rather small width, therefore reducing the overall width, of the resonance state c as compared to the width of the pure Stark state with quantum numbers $n=5$, $k=-2$. Additionally the resonance state c has contributions ranging from 0.1 to 8% of the parabolic state $n=4$, $k=-1$, which has the second smallest width out of the $n=4$ Stark manifold. Contributions from the parabolic state $n=6$, $k=-1$ are ranging from 0.5 to 3%. Our Stark analysis shows that the resonance states, although tending towards a specific parabolic state at large ion-surface distances, have a significant admixture of other Stark states at small and intermediate ion-surface distances.

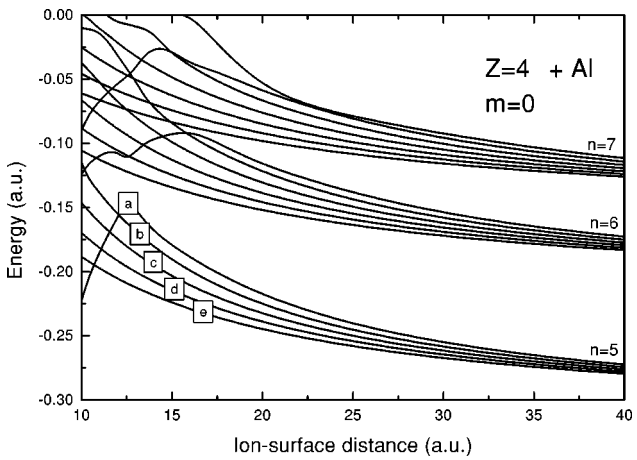

FIG. 7. Energies of the $m=0$ resonances states of the asymptotic $n=5$ to $n=7$ manifolds for a nuclear charge $Z=4$ near an Al surface. The labels $a-e$ refer to the widths in Fig. 8.

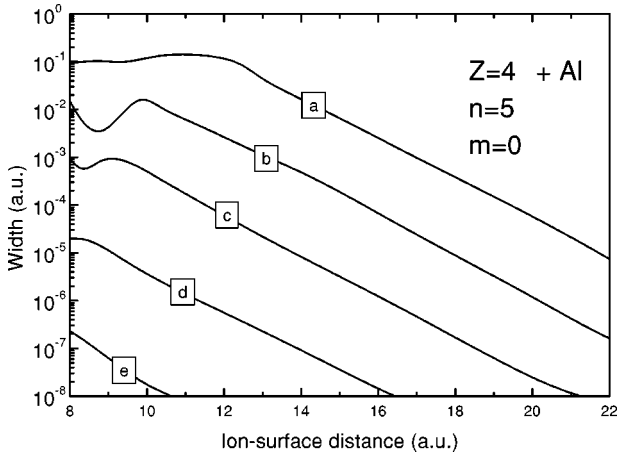

FIG. 8. Widths of the $n=5; m=0$ resonances states for a nuclear charge $Z=4$ near an Al surface. The labels $a-e$ refer to the energies in Fig. 7.

C. $Z=4$ + Al

Figures 7 and 8 show the energies and widths of $m=0$ resonance states for the nuclear charge $Z=4$ near an Al surface. The ionic basis set used was spanned by the $n=3$ to $n=9$ manifolds. The widths of resonance states denoted by $a-e$ in Fig. 7 are shown in Fig. 8. The individual resonance states have strikingly different widths. Comparing the energy diagram for $Z=4$ + Al (Fig. 7) with the diagram for $Z=3$ shown in Fig. 4 reveals that for a given n manifold around $Z=4$ the mixing with higher n manifolds takes place at smaller ion-surface distances. This is to be expected as the mean classical radius $\langle r_n \rangle = n^2/Z$ of Be^{3+} states is reduced by 3/4 as compared to Li^{2+}.

So far, we have shown results for $m=0$. In order to investigate the m dependence of resonance parameters, we show in Fig. 9 the $m=3$ resonance energies of the $n=5$ to $n=7$ manifolds and in Fig. 10 the widths of the $n=7$, $m=3$ manifold for the $Z=4$–Al surface system. The behavior in the shifts is similar to the shifts of the $m=0$ states being mainly driven by the repulsive nuclear image potential. The major difference is seen in the energetic downward shift

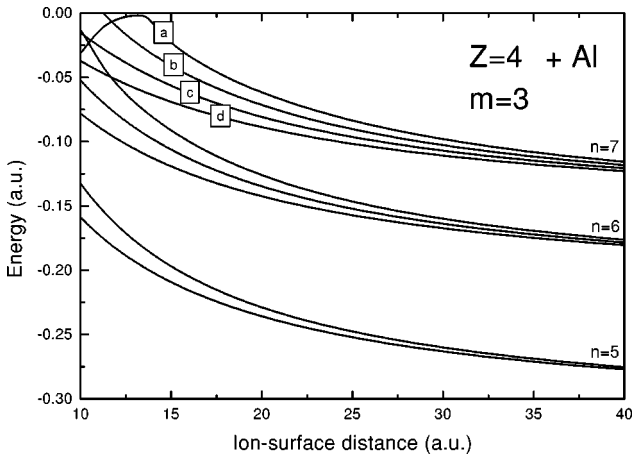

FIG. 9. Energies of the $m=3$ resonances states of the asymptotic $n=5$ to $n=7$ manifolds for a nuclear charge $Z=4$ near an Al surface. The labels $a-d$ refer to the widths in Fig. 10 and to the density plots shown in Figs. 11(a) to 11(d).

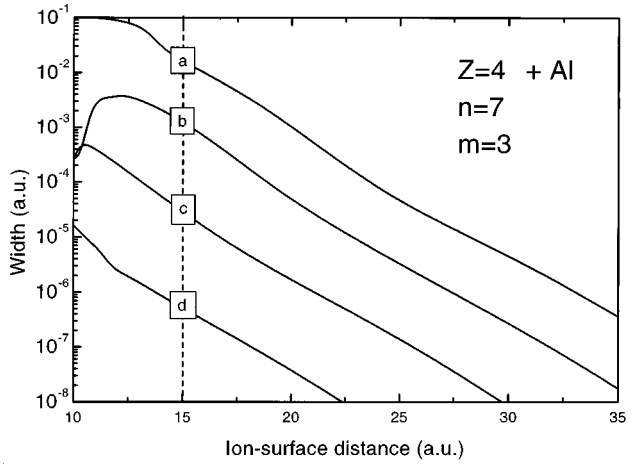

FIG. 10. Widths of the $n=7;m=3$ resonances states for a nuclear charge $Z=4$ near an Al surface. The labels $a-d$ and the vertical dashed line refer to the energies in Fig. 9 and density plots shown in Figs. 11(a)–11(d).

of resonance states, which tends to set in at smaller ion-surface distances as compared to the $m=0$ case. Since our quantization axis is perpendicular to the surface this behavior is to be expected as the probability density of high-m states tends to be oriented parallel to the surface, whereas the $m=0$ states tend to have their density pointing along the z axis perpendicular to the surface, therefore leading to a stronger interaction with the surface.

The hybridization of ionic orbitals according to Eq. (2.21) is presented in Figs. 11(a)–11(d) in which contour plots of the electronic probability density in a plane perpendicular to the surface including the ionic nucleus are shown. Displayed are the hybrid wave functions (2.21) for the asymptotic $n=7$, $m=3$ manifold. The ion-surface distance is 15 a.u., and we adopted a new reference frame with the ionic nucleus at the origin. The dashed line corresponds to the surface location. The labels $a-d$ refer to the shifts in Fig. 9 and widths presented in Fig. 10. While resonance a tends to point towards the surface, resonance d exhibits a charge density oriented towards the vacuum resulting in a decrease of the width by almost five orders of magnitude. The wave functions corresponding to the cases b and c are of moderate width and are somewhat symmetric with respect to reflection at an axis parallel to the surface and going through the nucleus.

In general, the shape of resonance wave functions changes as a function of the ion-surface distance. As an example for such an evolution Figs. 12(a)–12(c) show the previously discussed wave functions of resonance a, exhibiting

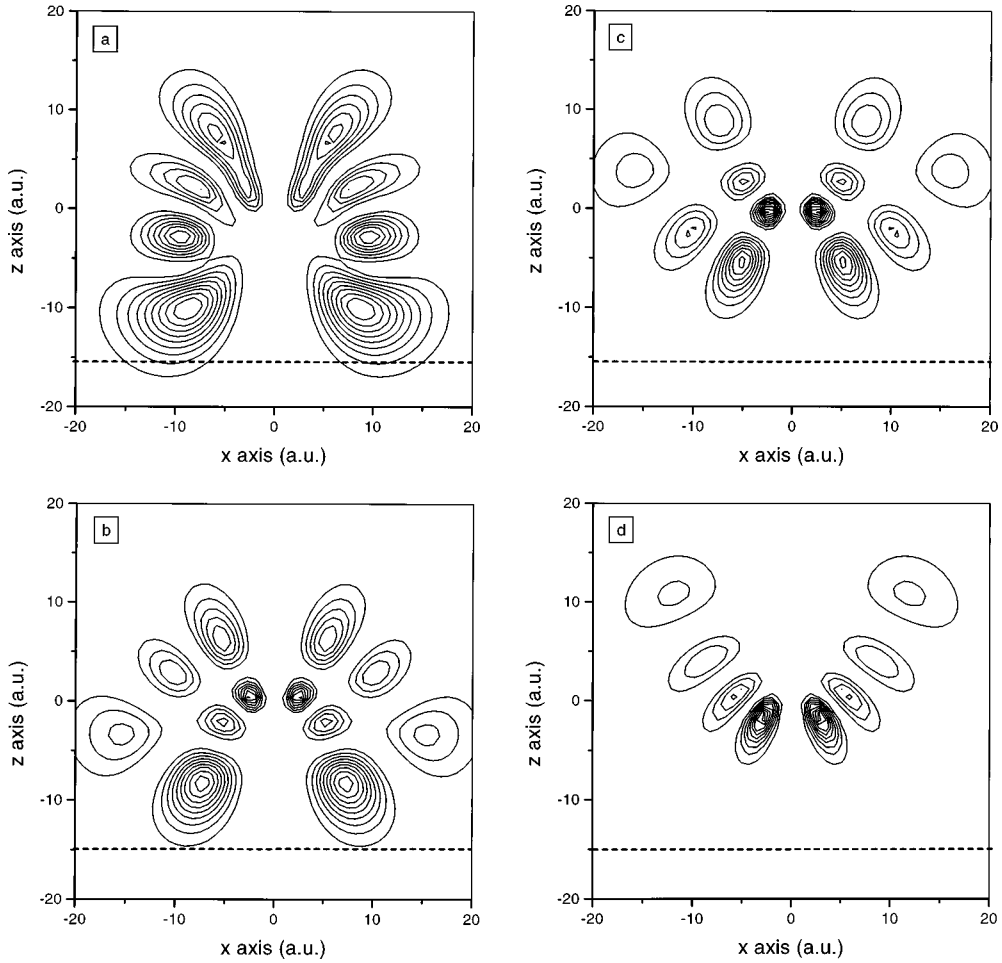

FIG. 11. (a)–(d) Contour plots of the charge density of the surface resonances in the plane perpendicular to the surface and containing the ionic nucleus of charge $Z=4$. The ion-surface distance is 15 a.u. and we used the ion-reference frame. The dashed line marks the surface edge. The labels (a)–(d) refer to the energies in Fig. 9 and widths in Fig. 10.

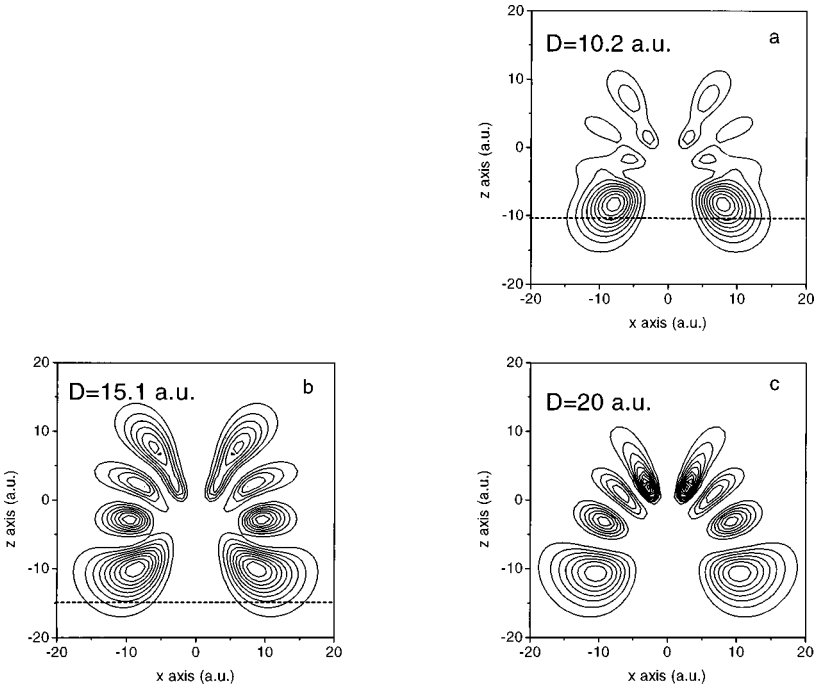

FIG. 12. (a)–(d) Contour plots of the charge density of the surface resonance exhibiting the largest width out of the asymptotic $n=7$, $m=3$ manifold. The distance between the ionic nucleus of charge $Z=4$ ranges from 10.2 to 20 a.u. The dashed line marks the surface edge.

the largest width in the asymptotic $n=7$, $m=3$ manifold, for ion-surface distances ranging from 10.2 to 20 a.u. It can be seen that, while approaching the surface, the density tends to bend towards the surface, which leads to a slight increase in the exponential slope of the corresponding width in the ion-surface distance range of 12.5 to 15 a.u. (cf. Fig. 10) and is related to the onset of the downward level shift (cf. Fig. 9). This illustrates that the change in shape of the resonance wave functions as a function of ion-surface distances leads to the nonadiabatic coupling among the surface resonances, which has to be taken into account when solving the time-dependent Schrödinger equation [27].

IV. CONCLUSION

The self-energy method used in the present work allows for the very efficient computation of surface resonances. Except for small ion-surface distances, the comparatively small set of bound hydrogenic basis states that need to be taken into account in order to generate converged results for level shifts and widths is roughly spanned by the n manifold of interest and neighboring manifolds. Similar to the molecular orbital method in slow ion-atom collisions, the method is ideally suited for the generation of surface resonances as basis functions for the solution of the time-dependent Schrödinger equation [27]. We have calculated accurate surface resonances formed during the slow encounter of an ion with a metal surface. Our results include resonance states around nuclear charges $Z=2$, 3, and 4 near an Al surface. While primarily investigating states with $m=0$, we showed that $m\neq 0$ states exhibit a similar behavior. For the case of He^+ and Li^{2+} interacting with an Al surface a comparison with two very different theoretical approaches yields reasonable agreement, and an analysis of the resonance states in terms of parabolic states shows that strong deviations from a Stark-like behavior occur at ion-surface distances smaller than the classical radius. Furthermore, we have related structural changes in the resonance density profile to characteristic changes in the resonance widths as a function of the ion-surface distance.

ACKNOWLEDGMENTS

We thank U. Wille for stimulating discussions. This work was supported by the Deutsche Forschungsgemeinschaft, through a grant for P.K., by the Division of Chemical Sciences, Basic Energy Sciences, Office of Energy Research, U.S. Department of Energy, by NSF Grant No. PHY-9604872, and by the Kansas Center for Advanced Scientific Computing (KSTAR) through the NSF/EPSCOR–KSTAR program.

[1] L. Folkerts, S. Schippers, D. M. Zener, and F. W. Meyer, Phys. Rev. Lett. **74**, 2204 (1995).
[2] H. Winter, Phys. Rev. A **46**, R13 (1992).
[3] C. Lemell, H. P. Winter, and F. Aumayr, Phys. Rev. A **53**, 880 (1996).
[4] J. Limburg, S. Schippers, I. G. Hughes, R. Hoekstra, R. Morgenstern, S. Hustedt, N. Hatke, and W. Heiland, Nucl. Instrum. Methods Phys. Res. B **98**, 436 (1995).
[5] J. W. Gadzuk, Surf. Sci. **6**, 159 (1966); **6**, 133 (1967).
[6] M. Remy, J. Chem. Phys. **53**, 2487 (1970).
[7] U. Thumm and J. S. Briggs, Nucl. Instrum. Methods Phys. Res. B **43**, 471 (1989).
[8] U. Thumm and J. S. Briggs, Nucl. Instrum. Methods Phys. Res. B **40/41**, 161 (1989); **47**, 476 (1990).

[9] U. Thumm, Ph.D. thesis, Universität Freiburg, 1989 (unpublished).
[10] U. Thumm, J. Phys. B **25**, 421 (1992).
[11] U. Wille, Phys. Rev. A **45**, 3004 (1992).
[12] U. Wille, Nucl. Instrum. Methods Phys. Res. B **100**, 303, (1995), and references therein.
[13] P. Kürpick and U. Thumm, Phys. Rev. A **54**, 1487 (1996).
[14] J. Burgdörfer, E. Kupfer, and H. Gabriel, Phys. Rev. A **35**, 4963 (1987).
[15] J. Burgdörfer, in *Review of Fundamental Processes and Applications of Atoms and Ions*, edited by C. D. Lin (World Scientific, Singapore, 1993), p. 517.
[16] P. Kürpick, U. Thumm, and U. Wille, Phys. Rev. A **56**, 543 (1997).
[17] P. Kürpick, U. Thumm, and U. Wille, Nucl. Instrum. Methods Phys. Res. B **125**, 273 (1997).
[18] A. G. Borisov, D. Teillet-Billy, and J. P. Gauyacq, Nucl. Instrum. Methods Phys. Res. B **78**, 49 (1993).
[19] A. G. Borisov and U. Wille, Surf. Sci. **338**, L875 (1995).
[20] A. G. Borisov, R. Zimny, D. Teillet-Billy, and J. P. Gauyacq, Phys. Rev. A **53**, 2457 (1996).
[21] P. Nordlander and J. C. Tully, Phys. Rev. B **42**, 5564 (1990); Phys. Rev. Lett. **61**, 990 (1988).
[22] P. Nordlander, Phys. Rev. B **53**, 4125 (1996).
[23] S. Deutscher, X. Yang, and J. Burgdörfer, Nucl. Instrum. Methods Phys. Res. B **100**, 336 (1995).
[24] S. Deutscher, X. Yang, J. Burgdörfer, and H. Gabriel, Nucl. Instrum. Methods Phys. Res. B **115**, 152 (1996).
[25] S. A. Deutscher, X. Yang, and J. Burgdörfer, Phys. Rev. A **55**, 466 (1997).
[26] F. Martín and M. F. Politis, Surf. Sci. **356**, 247 (1996).
[27] P. Kürpick, U. Thumm, U. Wille, Phys. Rev. A **57**, 1920 (1998).
[28] P. J. Jennings, R. O. Jones, and M. Weinert, Phys. Rev. B **37**, 6113 (1988).
[29] D. Park, Z. Phys. **159**, 155 (1960).